34th Annual International Conference of the IEEE EMBS
San Diego, California USA, 28 August - 1 September, 2012

Echogenicity in Transrectal Ultrasound is Determined by Sound Speed of Prostate Tissue Components

Hideki Tanoue, Yoshihiro Hagiwara, Kazuto Kobayashi, Yoshifumi Saijo, *Member, IEEE*

Abstract— **Typically, conventional transrectal ultrasound (TRUS) imaging of the cancer tissue is hypoechoic in echo texture. However, TRUS does not reliably distinguish between cancerous and non-cancerous tissue in the prostate. In the present study, sound speed of prostate needle biopsy specimens were measured by ultrasound speed microscope (USM) to construct a database for interpreting clinical TRUS images. Biopsy specimens were formalin-fixed and sectioned approximately 5 μm in thickness. They were mounted on glass slides without cover slips. The ultrasonic transducer with the central frequency of 120 MHz was mechanically scanned over the specimen to measure sound speed distribution. Echo intensity of TRUS images were qualitatively classified into three categories; hyperechoic, iso-echoic and hypoechoic areas. Sound speed was 1596.9 ± 28.2 m/s in hyperechoic, 1571.2 ± 35.8 m/s in iso-echoic and 1562.6 ± 35.1 m/s in hypoechoic area, respectively. However, echo intensity showed no significant relationship to malignancy of prostatic tissue. Echo intensity of TRUS is significantly affected with tissue components and USM findings would provide important information for interpretation of TRUS images.**

I. Introduction

TYPICALLY, the prostatic cancer tissues proven by histological examination were hypoechoic in transrectal ultrasound (TRUS) imaging. Areas of moderate echogenicity were found to be secondary to ingrowth of tumor into the central area of benign hyperplastic tissue [1]. However, TRUS does not reliably distinguish between cancerous and non-cancerous tissue in the prostate; therefore, TRUS-guided biopsies simply use typically well-imaged anatomical structures, such as the interface between the gland and periprostatic fibroadipose tissues, as a spatial reference for placing core needles in the gland. Recently, new methods of tissue-type imaging that are based on spectrum analysis of echo signals and that utilize artificial neural networks for classification offer better reliably distinguishing cancerous lesions from non-cancerous tissue in the prostate than conventional echography [2].

The ultrasonic properties of various tissues and cells have been investigated by scanning acoustic microscopy (SAM) since 1980s [3-13]. SAM provides basic data for understanding clinical ultrasound images with lower frequency ultrasound. Recently, ultrasound speed microscope (USM) which measures two-dimensional distribution of sample thickness and sound speed has been used for medicine and biology. USM uses a single pulsed wave instead of burst waves used in conventional SAM systems [14-17]. In the present study, sound speed of core-needle biopsied prostate tissues are measured by USM and the relation between echogenicity and sound speed of prostate tissue is discussed.

II. Methods

A. Instrumental Setup

An electric impulse was generated by a high speed switching semiconductor. The start of the electric pulse was within 400 ps from excitation, the pulse width was 2 ns, and the pulse voltage was 40 V. The electric pulse was input to a concave transducer with the copolymer of vinylidene fluoride and trifluoroethylene P(VDF-TrFE) used as the active element. The aperture diameter of the transducer was 1.2 mm, and the focal length was 1.5 mm. The center frequency was 120 MHz, the bandwidth (-6 dB) was 60-170 MHz, and the pulse repetition rate was 10 kHz. The diameter of the focal spot was estimated to be 15 μm at 100 MHz by taking into account the focal distance and sectional area of the transducer.

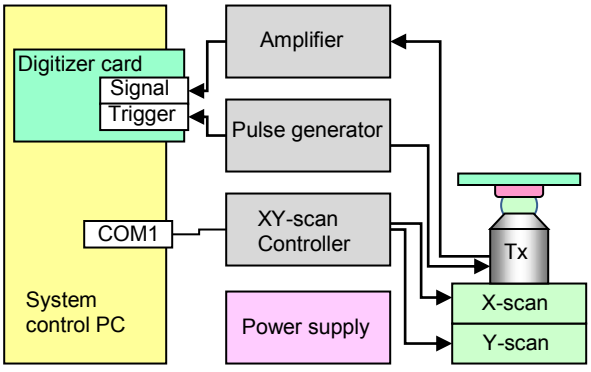

Fig. 1. Block diagram of ultrasound speed microscope (USM)

Fig. 1 shows a block diagram of the USM for biological

Manuscript received March 14, 2012. This project was supported in part by Grants-in-Aid for Scientific Research (Scientific Research (B) 22300175, Challenging Exploratory Research 23650300) from the Japan Society for the Promotion of Science, Sendai Advanced Preventive Health Care Services Cluster from the Ministry of Education, Culture, Sports, Science and Technology and Regional Innovation Program from the Ministry of Economy, Trade and Industry.

Hideki Tanoue is with the Graduate School of Biomedical Engineering, Tohoku University, Sendai 980-8579 Japan (e-mail: ypoons1950@nifty.com).

Yoshihiro Hagiwara is with the Graduate School of Medical Sciences, Tohoku University, Sendai 980-8575 Japan (e-mail: hagi@dent.tohoku.ac.jp).

Kazuto Kobayashi is with the Honda Electronics Co. Ltd., Toyohashi 441-3193 Japan (e-mail: kazuto@honda-el.co.jp).

Yoshifumi Saijo is with the Graduate School of Biomedical Engineering, Tohoku University, Sendai 980-8579 Japan (phone: +81-22-717-8514; fax: +81-22-795-5882; e-mail: saijo@idac.tohoku.ac.jp).

tissue characterization. Saline (0.9%) was used as the coupling medium between the transducer and the specimen. Temperature was maintained as 20 °C during whole measurements. The reflections from the tissue surface and those from the interface between the tissue and glass were received by the transducer and were introduced into a Windows-based PC with a fast digitizer card (Acqiris DP1400, onboard memory 16MB, Geneva, Switzerland). The frequency range was 500 MHz, and the sampling rate was 2 GS/s. Eight consecutive values of the signal taken for a pulse response were averaged in order to reduce random noise.

The transducer was mounted on an X-Y stage driven by a XY-scan controller with a microcomputer board that was controlled by the PC through RS232C. The both X-scan and Y-scan were driven by linear servo motors and the position was detected by an encoder. The scan was controlled to reduce the effects of acceleration at the start and deceleration at the end of the X-scan. Finally, two-dimensional distributions of ultrasonic intensity, speed of sound, attenuation coefficient and thickness of a specimen measuring 2.4×2.4 mm were visualized using 300×300 pixels. The total scanning time was 63 s.

B. Signal Analysis

Fig. 2 shows the schematic illustration of reflections. The distance from the transducer to the glass surface was 1.5 mm. Reflected wave contained two components of reflections from the surface of the tissue (S_{front}) and the interface between the tissue and glass (S_{rear}). The phase of the waveforms from the tissue and glass were standardized by a reflection from the glass (S_{ref}) of the same scanning line.

Denoting the standardized phase of the reflection wave at the tissue surface as ϕ_{front}, the standardized phase at the interference between the tissue and the substrate as ϕ_{rear},

$$2\pi f \times \frac{2d}{c_o} = \phi_{front} \qquad (1)$$

$$2\pi f \times 2d\left(\frac{1}{c_o} - \frac{1}{c}\right) = \phi_{rear} \qquad (2)$$

where d is the tissue thickness, c_o is the sound speed in coupling medium and c is the sound speed in the tissue.

Thickness is obtained as

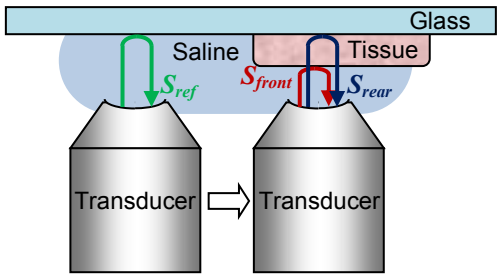

Fig. 2. Schematic illustration of the reflections at tissue and glass

$$d = \frac{c_o}{4\pi f}\phi_{front} \qquad (3)$$

Finally, sound speed is calculated as

$$c = \left(\frac{1}{c_o} - \frac{\phi_{rear}}{4\pi fd}\right)^{-1} \qquad (4)$$

After determination of the thickness, attenuation of ultrasound at 120 MHz was then calculated by dividing amplitude by the thickness.

C. Sound Speed and Reflection

Generally, density ρ and sound speed c determine the characteristic acoustic impedance Z of the material as

$$Z = \rho c$$

On the assumption that the interface between two fluid-like media (medium a and medium b) is infinite and plane, the relative reflected sound power, in dB, can be determined by the specific acoustic impedance of each medium as

$$dB = 10\log_{10}\frac{P_r}{P_i} = 10\log_{10}\frac{(Z_a - Z_b)^2}{(Z_a + Z_b)^2}$$

(P_r: sound power reflected at interface, P_i: incident sound power, Z_a: acoustic impedance of medium a, Z_b: acoustic impedance of medium b)

D. Prostate Biopsy Tissues

Prostate tissue was obtained by TRUS guided biopsy. All biopsy results were reviewed and assigned a Gleason score.

All patients involved in this study (n=29) provided written informed consent. Biopsied specimens from patients were fixed by 4% formaldehyde overnight, and embedded in paraffin by using standard processing for histology. The paraffin blocks were stored in a refrigerator at 5 °C. The samples for the acoustic microscopy were de-paraffinized without staining for acoustic microscopy. The neighboring section for USM was stained with Hematoxylin-Eosin staining for optical microscopy.

E. Transrectal Ultrasound (TRUS)

TRUS images were obtained by a conventional ultrasound machine (ALOKA, SSD3500, Tokyo, Japan) and a transrectal ultrasound probe with the central frequency of 5.0 MHz. Echo movie was recorded on VHS video tape during core-needle biopsy procedures. All the ultrasound parameters were maintained at the same setting. Echo image was captured by a frame grabber for semi-quantitative analysis of echo intensity. Echogenisity was classified into three categories; hyperechoic, iso-echoic and hypoechoic areas compared to the intensity in normal appearance region.

III. Results

Fig. 3 shows an example of the TRUS image showing high intensity echo (A), histology (B) and USM image (C) of the biopsied sample. The sound speed is 1580 m/s and the tissue was proven as moderately differentiated adenocarcinoma.

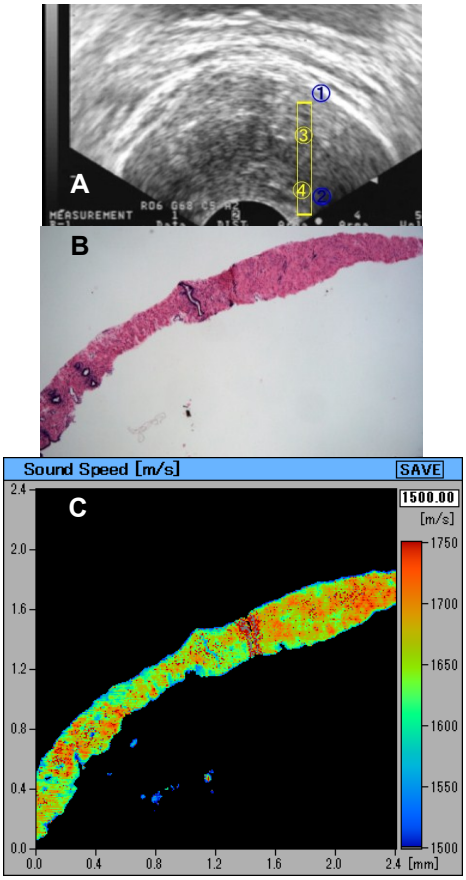

Fig. 3. Moderately differentiated adenocarcinoma. (A) TRUS image, (B) optical image, (C) USM image

Fig. 4 shows an example of the TRUS image showing mixture of high and low intensity echo (A), histology (B) and USM image (C) of the biopsied sample. The histology was proven as poorly differentiated carcinoma.

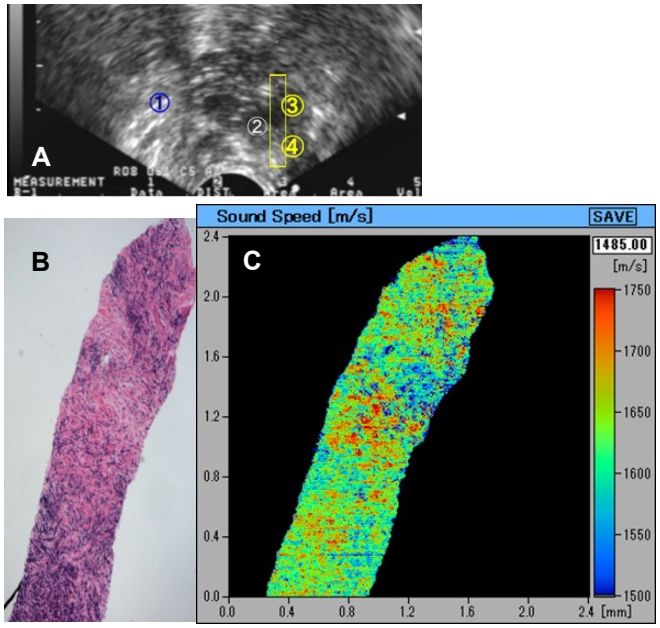

Fig. 4. Poorly differentiated adenocarcinoma. (A) TRUS image, (B) optical image, (C) USM image

Fig. 5 shows a scattered graph of the sound speed categorized by echo intensity. 106 regions from 29 patients were plotted. Mean and standard deviation value of the sound speed was 1596.9 ± 28.2 m/s in hyperechoic area, 1571.2 ± 35.8 m/s in isoechoic area and 1562.6 ± 35.1 m/s in hypoechoic area, respectively. These values showed significant difference between each other ($p<0.05$, Mann-Whitney's U test).

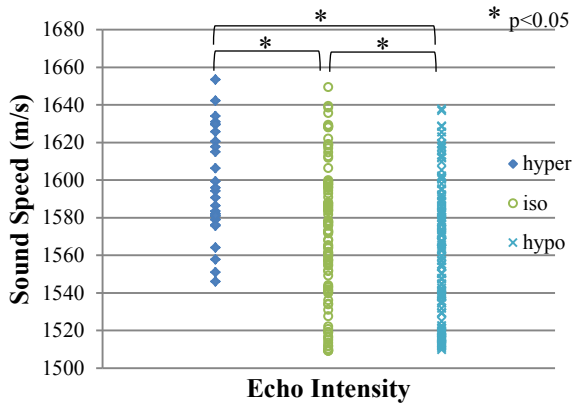

Fig. 5. Scattered graph of the sound speed categorized by echo intensity.

Fig. 6 shows the bar graph showing mean and standard deviation of sound speed in each cancer type and tissue components of the normal prostate. The sound speed of well-differentiated tubular adenocarcinoma was significantly lower than those of moderately differentiated adenocarcinoma or poorly differentiated adenocarcinoma ($p<0.05$, Student's T-test), but the difference was much smaller than the difference between tissue type (for example, interstitial tissue and cystic tissue).

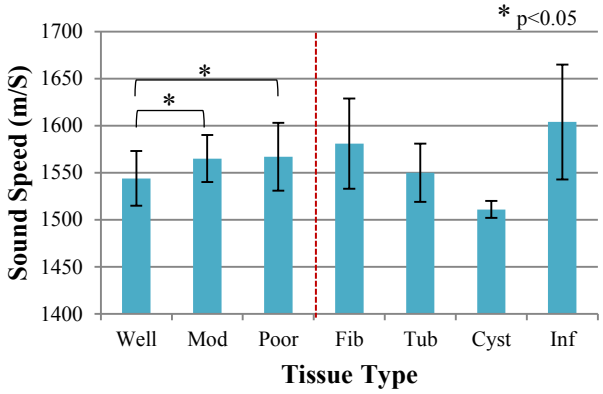

Fig. 6. Bar graph of the sound speed in cancer and tissue type.
Well: well-differentiated tubular adenocarcinoma
Mod: moderately differentiated adenocarcinoma
Poor: poorly differentiated adenocarcinoma
Fib: fibrosis
Tub: normal tubular structure
Cyst: cystic lesion
Inf: inflammation

IV. Discussion

USM has enabled the measurement of sound speed at microscopic level. Values of the specific acoustic impedance depend on the sound speed because the density of the biological soft tissues does not differ significantly. Although the properties of the high frequency focused ultrasound used in USM measurement may be different from that used in lower frequency TRUS device, the sound speed strongly influenced TRUS echogenicity. The sound speed of the interstitial tissue was higher than the normal tubular structure or cystic lesion. Benign prostate hypertrophy often showed hyperechoic echo in TRUS and high sound speed in USM image. In such case, the tissue contains much fibrosis and less tubular structure.

In the present study, TRUS and needle biopsy procedures were performed in routine clinical settings. Thus, the TRUS image was qualitative. Quantitative TRUS and sound speed measurement by USM should be compared to understand the mechanisms of echogenicity in the future.

V. Conclusions

Ultrasound speed microscope (USM) was equipped in order to assess the echogenicity in TRUS images. The results indicate sound speed of the tissue strongly influenced the echogenicity while smaller differences were observed between benign and malignant tissues. These results help understanding the intensity and texture of prostate cancer in clinical diagnosis.

References

[1] F. Lee, J.M. Gray, R.D. McLeary, T.R. Meadows, G.H. Kumasaka, G.S. Borlaza, W.H. Straub, F. Lee, Jr., M.H. Solomon, T.A. McHugh, R.M. Wolf, Transrectal ultrasound in the diagnosis of prostate cancer: Location, echogenicity, histopathology, and staging, *The Prostate*, 7 (1985), pp. 117-129.

[2] E. J. Feleppa, Ultrasonic tissue-type imaging of the prostate: Implications for biopsy and treatment guidance, *Cancer Biomarkers* 4 (2008), pp. 201-212.

[3] M. Tanaka, H. Okawai, N. Chubachi, J. Kushibiki, T. Sannomiya, Propagation properties of ultrasound in acoustic microscopy through a double-layered specimen consisting of thin biological tissue and its holder, *Jpn J Appl Phys* 23 (1984), pp. 197-199.

[4] Y. Saijo, M. Tanaka, H. Okawai, F. Dunn, The ultrasonic properties of gastric cancer tissues obtained with a scanning acoustic microscope system, *Ultrasound Med Biol* 17 (1991), pp. 709-714.

[5] A. F. van der Steen, M. H. Cuypers, J. M. Thijssen, P. C. de Wilde, Influence of histochemical preparation on acoustic parameters of liver tissue: a 5-MHz study, *Ultrasound Med Biol* 17 (1991), pp. 879-91.

[6] G. A. Briggs, J. Wang, R. Gundle, Quantitative acoustic microscopy of individual living human cells, *J Microsc* 172 (1993), pp.3-12.

[7] H. Sasaki, M. Tanaka, Y. Saijo, H. Okawai, Y. Terasawa, S. Nitta, K. Suzuki, Ultrasonic tissue characterization of renal cell carcinoma tissue, *Nephron* 74 (1996), pp. 125-130.

[8] Y. Saijo, M. Tanaka, H. Okawai, H. Sasaki, S. Nitta, F. Dunn, Ultrasonic tissue characterization of infarcted myocardium by scanning acoustic microscopy, *Ultrasound Med Biol* 23 (1997), pp. 77-85.

[9] Y. Saijo, H. Sasaki, H. Okawai, S. Nitta, M. Tanaka, Acoustic properties of atherosclerosis of human aorta obtained with high-frequency ultrasound, *Ultrasound Med Biol* 24 (1998), pp. 1061-1064.

[10] J. Bereiter-Hahn, H. Lüers, Subcellular tension fields and mechanical resistance of the lamella front related to the direction of locomotion, *Cell Biochem Biophys* 29 (1998), pp. 243-62.

[11] Y. Saijo, H. Sasaki, M. Sato, S. Nitta, M. Tanaka, Visualization of human umbilical vein endothelial cells by acoustic microscopy, *Ultrasonics* 38 (2000), pp. 396-399.

[12] Y. Saijo, T. Ohashi, H. Sasaki, M. Sato, C.S. Jorgensen, S. Nitta, Application of scanning acoustic microscopy for assessing stress distribution in atherosclerotic plaque, *Ann Biomed Eng* 29 (2001), pp. 1048-53.

[13] H. Sasaki, Y. Saijo, M. Tanaka, S. Nitta, Influence of tissue preparation on the acoustic properties of tissue sections at high frequencies, *Ultrasound Med Biol* 29 (2003), pp. 1367-72.

[14] N. Hozumi, R. Yamashita, C.K. Lee, M. Nagao, K. Kobayashi, Y. Saijo, M. Tanaka, N. Tanaka, S. Ohtsuki, Time-frequency analysis for pulse driven ultrasonic microscopy for biological tissue characterization, *Ultrasonics* 42 (2004), pp. 717-722.

[15] Y. Saijo, N. Hozumi, K. Kobayashi, N. Okada, E. D. Santos Filho, H. Sasaki, T. Yambe, M. Tanaka, Ultrasonic tissue characterization of atherosclerosis by a speed-of-sound microscanning system, *IEEE Trans Ultrason Ferroelectr Freq Control* 54 (2007), pp. 1571-1577.

[16] Y. Hagiwara, A. Ando, E. Chimoto, Y. Saijo, K. Ohmori-Matsuda, E. Itoi, Changes of articular cartilage after immobilization in a rat knee contracture model, *J Orthop Res* 27 (2009), pp. 236-242.

[17] H. Tanoue, Y. Hagiwara, K. Kobayashi, Y. Saijo, Ultrasonic tissue characterization of prostate biopsy tissues by ultrasound speed microscope, *Conf Proc IEEE Eng Med Biol Soc. 2011* (2011), pp. 8499-8502.